

UNDERSTANDING PHOTOSYNTHESIS IN A SALT MARSH USING OBSERVATIONS OF SOLAR-INDUCED CHLOROPHYLL FLUORESCENCE

Hannah M. Mast¹, Koong Yi¹, Sally E. Pusede¹, and Xi Yang¹
¹Department of Environmental Sciences, University of Virginia

Abstract

Despite their small areal extent, salt marshes serve as a large carbon sink, sequestering carbon through efficient photosynthesis and carbon burial. Quantifying gross primary production (GPP) in an intertidal marsh is complicated by tidal cycles because few methods can measure photosynthesis in all stages of tidal inundation or at large spatial scales. Remote sensing of solar-induced chlorophyll fluorescence (SIF) is a promising approach to address these challenges. SIF is emitted by photosynthetic molecular machinery and has been shown to directly correlated with GPP in multiple ecosystem types. Here, I describe concurrent measurements of SIF using an automated spectrometer system and eddy covariance (EC) measurements for the 2020 growing season in a salt marsh on the Virginia Eastern Shore. I identify diurnal, tidal, and seasonal patterns in SIF and examine how these patterns are modulated by environmental factors. Our preliminary results have shown a clear diurnal pattern of SIF at 760 nm peaking at midday with maximum intensities reaching $1.5 \text{ mW m}^{-2} \text{ sr}^{-1} \text{ nm}^{-1}$. I also investigate relationships between SIF and EC-derived GPP during different stages of inundation in order to improve estimates of GPP at high tides when EC may not yield reliable results.

Introduction

Forecasting the global carbon budget in the context of climate change requires accurate estimates of the exchange of carbon dioxide (CO_2) between the atmosphere, vegetation, and the ocean, and how these fluxes will be altered by climate change. Coastal ecosystems play an outsized role in the global carbon cycle and

account for 50% of ocean organic carbon burial, in spite of covering only 0.2% of the ocean's surface.¹ Salt marshes sequester up to $200 \text{ g C m}^{-2} \text{ yr}^{-1}$, orders of magnitude larger than the rates of tropical forests.²

Rates of photosynthesis for salt marsh vegetation are typically measured *in situ*; therefore, observations are limited in spatial coverage to just a tiny fraction of total global wetland areas. Landscape-scale estimates of gross primary production (GPP), the total

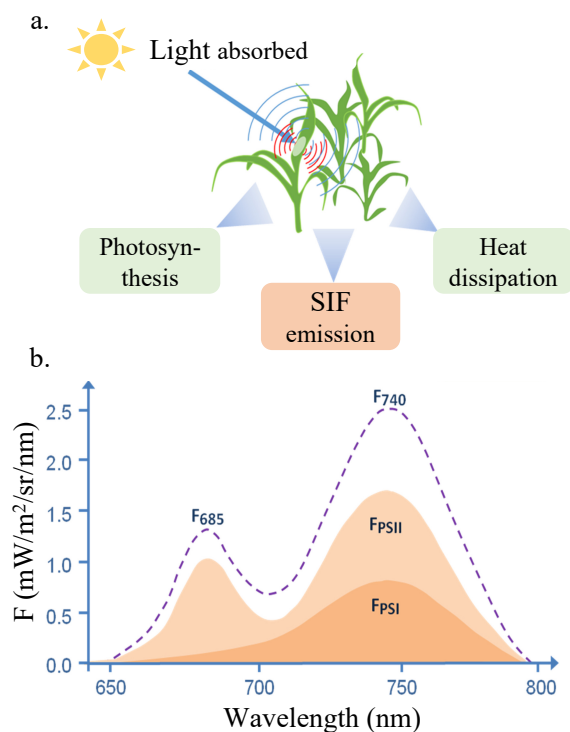


Figure 1: Schematic illustrating partitioning of absorbed photons between photosynthesis, heat dissipation, and SIF emission (a). Fluorescence spectrum of SIF spans 650-800nm with peaks at 685 and 749 nm from photosystem I and II (b). Figure adapted from Mohammed *et al.*, 2019.

carbon uptake by vegetation, can be obtained with eddy covariance (EC), a well-established technique based on correlations between deviations in the mean vertical wind speed and CO₂ mixing ratios to estimate land-atmosphere exchange of CO₂.³ Previous studies using EC have found photosynthesis to decrease when salt marsh vegetation is inundated.⁴ However, it is challenging to estimate GPP with EC when vegetation is inundated because the tide incorporates another source/sink of CO₂, and additional independent approaches are needed. Thus, estimates of salt marsh carbon stocks at landscape to regional scales remain highly uncertain due to a lack of measurements that can capture high spatial and temporal variability and measure photosynthesis both above and below water levels.⁵

Remote sensing is a promising approach to capture larger spatial and temporal trends of photosynthesis but has its own challenges. Traditional remote sensing methods rely on vegetation indices, such as the Normalized Difference Vegetation Index (NDVI), as a proxy for GPP and likely do not fully capture the spatial and temporal variations in photosynthesis. Furthermore, coastal ecosystems are especially challenging to study with satellite observations without local ground-based measurements, as wetlands are often narrower than satellite pixels.

Solar-induced chlorophyll fluorescence is a promising approach to directly measure photosynthesis and has recently become possible to observe with remote sensing at the Earth's surface and from satellites. While most of the incident solar radiation absorbed by a leaf is partitioned to photosynthesis or dissipated as heat, excited chlorophyll molecules fluoresce 1-2% of the absorbed photons as SIF (Figure 1a).^{6,7} The SIF intensity has been empirically shown to be proportional to the rate of the electron transport chain in photosynthesis and to correlate with GPP at the canopy scale.^{8,9} At the leaf level, wavelengths of SIF emission span the red (SIF_R) and far-red



Figure 2: Map of Virginia Coast Reserve with star marking location of study site.

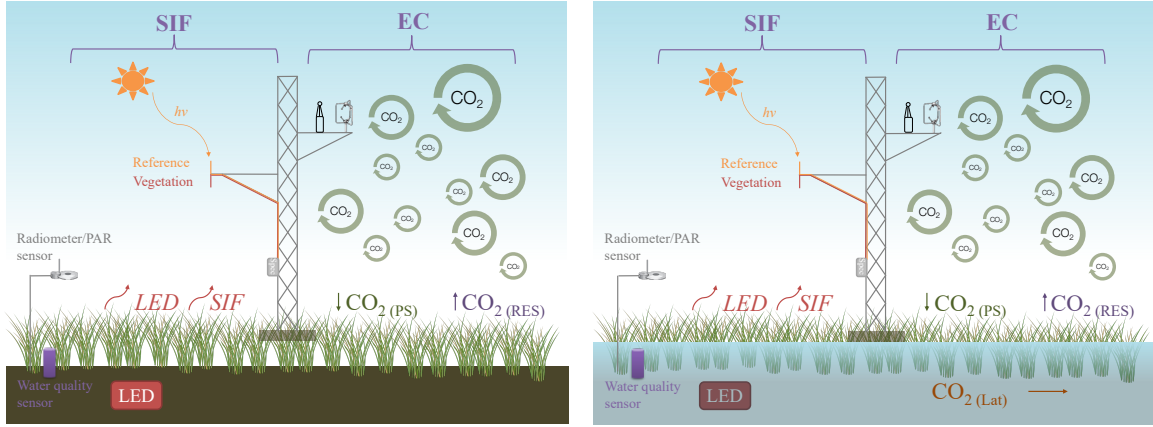
(SIF_{FR}) regions of the electromagnetic spectrum (650-800 nm), with two peaks of fluorescence at 685 and 740 nm (Figure 1b).

In contrast to EC, the large swath of SIF emission wavelengths make it uniquely suited to measure photosynthesis across all tidal conditions. Terrestrial ecologists tend to measure SIF_{FR} due to strong reabsorption in the SIF_R region by photosynthetic pigments within dense canopies.¹⁰ Oceanographers utilize SIF_R to study phytoplankton productivity because water strongly absorbs light in the infrared region.¹¹

Here, I present the first SIF observations of salt marsh vegetation and an approach to estimate GPP across tidal conditions with co-measured EC on Virginia's Eastern Shore. I also examine potential environmental controls of SIF and GPP at the scale of a single marsh.

Methods

All data was collected at the Virginia Coast Research on the eastern shore of Virginia, USA at the Fowling Point salt marsh (37° 24' N, 75° 50' W, Figure 2). The marsh is dominated by



Low Tide

$$CO_{2(Net)} = CO_{2(Res)} - CO_{2(PS)} \quad (1a)$$

$$SIF_{Obs} = SIF_{Canopy} \quad (2a)$$

$$SIF_{Obs} = SIF_{Canopy} + LED \quad (3a)$$

High Tide

$$CO_{2(Net)} = CO_{2(Res)} - CO_{2(PS)} \pm CO_{2(Lat)} \quad (1b)$$

$$SIF_{Obs} = SIF_{Canopy} \left(\frac{1}{a}\right) \quad (2b)$$

$$SIF_{Obs} = SIF_{Canopy} \left(\frac{1}{a}\right) + LED \left(\frac{1}{a}\right) \quad (3b)$$

Figure 3: Experimental design at low and high tide conditions. Equations 1a and 1b represent eddy covariance CO_2 balance; Equations 2a and 2b represent SIF no LED light condition while Equations 3a and 3b illustrate SIF when the LED is on. Res=respiration, PS=photosynthesis, Lat=lateral, Obs=observed, a=light attenuation from water and plants.

Spartina alterniflora smooth cordgrass and inundated by the tide twice a day.

SIF was measured in the fluorescence emission wavelength range (650-800 nm) with the FluoSpec 2 system as described by Yang *et al.* (2018) during the 2020 and 2021 growing seasons.¹² Red and far-red high-resolution spectrometers (QEpro, OceanOptics) were connected to an inline fiber optic shutter (FOS-2x2-TTL, OceanOptics) with two ports, each of which was connected to a fiber optic. The fibers were mounted 5 m above the marsh canopy, with one pointed down to measure canopy radiance and one was connected to a cosine corrector (CC-3, OceanOptics) and directed to the sky to collect irradiance from 180° FOV. The shutter switched between fibers to alternate measurements from either the sky or vegetation, with the sky radiance serving as a reference for the subsequent canopy radiance measurement. The raw spectrometer data was converted to irradiance ($mW m^{-2} nm^{-1}$) and radiance ($mW m^{-2} sr^{-1} nm^{-1}$) as described by Perez-Priego *et al.* (2005) and averaged to 30

minutes in order to compare to EC.¹³ All measurements were corrected for dark current. Radiometric and wavelength calibrations were performed with a radiometric calibration light source (HL-3P-CAL, OceanOptics) and a wavelength calibration light source (HG-2, OceanOptics) each spring.

The FluoSpec 2 system has been validated in terrestrial ecosystems, but it may not reliably measure SIF at high tides when water can attenuate the signal. To address this issue, an LED light calibration experiment was used to build a correction model for vegetation-based SIF that adjusts for the current tidal level.¹⁴ The LED light source (#ELD-740-524, Roithner Lasertechnik) emitted light in the SIF infrared and red regions and served as a reference to determine a SIF signal attenuation factor (a) for a given water level when vegetation is partially submerged. SIF observed at the sensor (SIF_{obs}) could thus be corrected to more closely reflect SIF of the canopy (SIF_{canopy}) (Equations 2 and 3, Figure 3).

Net marsh-atmosphere ecosystem exchanges (NEE) of CO₂ and H₂O were measured with EC at 20 Hz using a Licor 7500DS IRGA and Gill WindMaster sonic anemometer and averaged over 30 minute periods. Instruments were mounted on a tower 3.7 m above the marsh surface and measured from May 2019 through the 2021 growing season. Webb-Pearman-Leuning, sonic temperature, and frequency response corrections were applied to the raw data.^{15,16} A nighttime friction velocity was applied before partitioning the net CO₂ into GPP and respiration components by modeling respiration as a function of temperature.

Next, low-tide periods were used to determine the slope of the linear fit between SIF_{canopy} and EC-derived GPP flux. The SIF_{canopy}-GPP relationship was then extrapolated to high tide conditions when EC does may not yield reliable results. I applied this method across the 2020 and 2021 growing seasons to estimate annual GPP.

Additional environmental variables were measured at the site to examine potential environmental controls of SIF and GPP. Upwelling and downwelling short and long wave radiation was measured with a net radiation sensor (CNR4, Kipp & Zonen). Photosynthetically active radiation (PAR) was monitored with a PAR sensor (PQS1, Kipp & Zonen). Local tidal depth data was obtained from NOAA's public mean high high water (MHHW) dataset at Wachapreague, VA (Station ID: 8631044) that is nearby the field site and known to experience the same tidal conditions.

Preliminary Results

Preliminary EC NEE fluxes show a clear diurnal and seasonal pattern of greater CO₂ uptake by the marsh at midday and during the summer months (Figure 4 and 6a). SIF_{FR} follows a similar diurnal and seasonal pattern, with fluorescence at 760 nm peaking at midday at maximum intensities reaching up to 1.5 mW

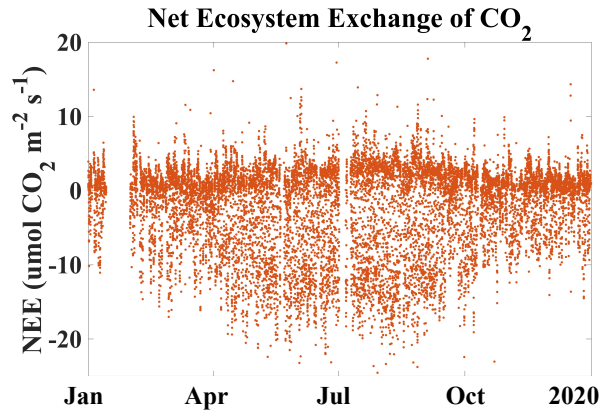


Figure 4: Net ecosystem exchange (NEE) of CO₂ measured with eddy covariance in 2020.

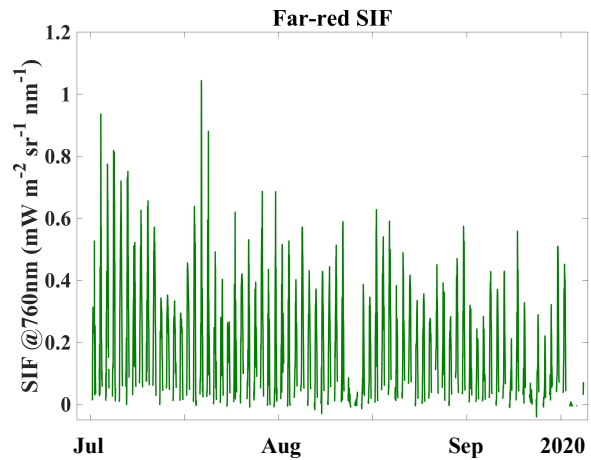


Figure 5: SIF emission in the far-red emission region at 760 nm in Summer 2020.

m² sr⁻¹ nm⁻¹ and emission continuing well into September (Figure 5 and 6b).

Differences in the relationship between NEE and SIF_{FR} arise when data is binned by tidal conditions (Figure 7). When comparing across all MHHW, SIF_{FR} and NEE have an exponential decay $R^2 = 0.2681$. The correlation increases to $R^2 = 0.3916$ when filtered for the lowest 25 percentile MHHW, and it decreases to $R^2 = 0.1201$ during the highest 25 percentile tides. Notably, large SIF_{FR} values continue during high tide conditions while NEE fluxes shift towards zero.

Discussion and Next Steps

Our preliminary results suggest SIF_{FR} can continue to escape the canopy during high tidal conditions, suggesting SIF may track photosynthesis even as the water's surface modulates gas exchange measured by EC. This is especially interesting considering that light in the far-red region should be strongly absorbed by water and previous studies found photosynthesis to diminish during high tides.

Our immediate next steps are to partition the EC NEE flux into GPP and respiration components to have more direct comparison to SIF. Next, I will analyze SIF_R with a focus on how red SIF emission differs across tidal conditions compared to SIF_{FR} and EC-derived GPP.

In spring-summer 2021, I will complete the LED light calibration light experiment to obtain SIF signal attenuation factors and allow us to better model SIF under different tidal conditions. I can then move to understanding relationships between SIF_{canopy} and GPP at low tides before extrapolating to high tidal conditions.

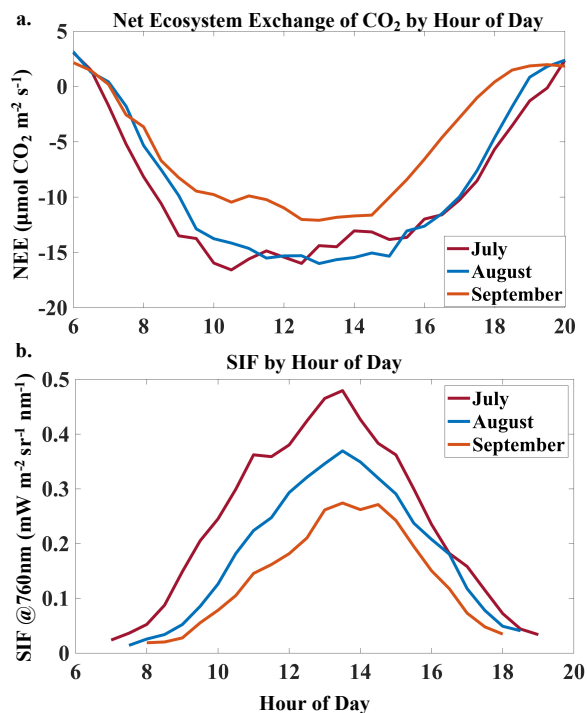


Figure 6: Net ecosystem exchange (NEE) of CO₂ (a) and far-red SIF at 760 nm (b) averaged by hour of day in Summer 2020.

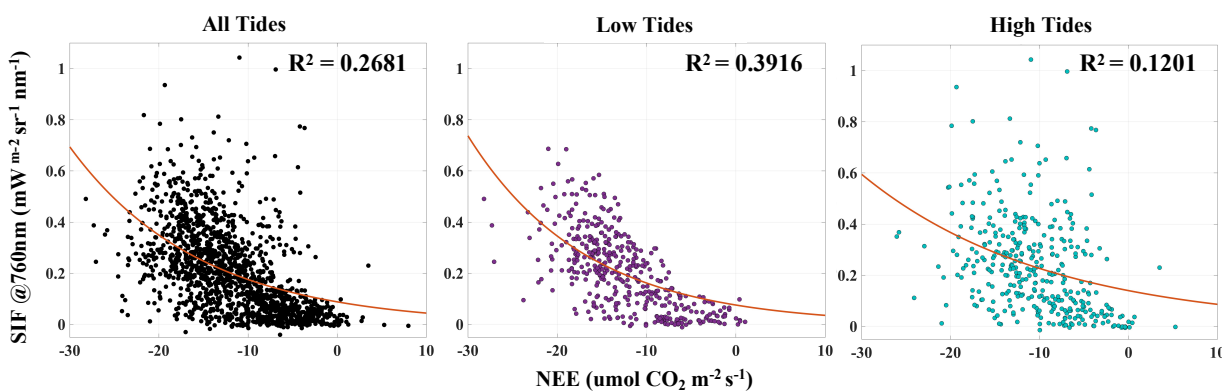


Figure 7: Comparing far-red SIF and daytime net ecosystem exchange (NEE) of CO₂ at all tides (a), low tides when MHHW <25 percentile (b), and high tides when MHHW >25 percentile. Data was fit to exponential decay equation $f(x) = a \cdot \exp(b \cdot x)$. All tides: $a=0.08847$, $b=-0.06867$. Low tides: $a=0.07595$, $b=-0.07578$. High tides: $a=0.1402$, $b=-0.04817$.

Acknowledgements

I thank John Porter for data management and technical support, Chris So for site design and assembly, and all Pusede Lab and Yang Lab members.

References

1. Duarte C.M. 2017. Reviews and syntheses: Hidden forests, the role of vegetated coastal habitats in the ocean carbon budget. *Biogeosciences* 14:301-310.
2. McLeod E., Chmura G.L., Bouillon S., Salm R., Björk M., Duarte C.M., Lovelock C.E., Schlesinger W.H., Silliman B.R. 2011. A blueprint for blue carbon: toward an improved understanding of the role of vegetated coastal habitats in sequestering CO₂. *Front Ecol Environ* 9:552-560.
3. Baldocchi D.D., Hincks B.B., Meyers T.P. 1988. Measuring Biosphere-Atmosphere Exchanges of Biologically Related Gases with Micrometeorological Methods. *Ecology* 69(5): 1331-1340.
4. Kathilankal J.C., Mozdzer T.J., Fuentes J.D., D'Odorico P., McGlathery K.J., Ziemann J.C. 2008. Tidal influences on carbon assimilation by a salt marsh. *Environ. Res. Lett.* 3 044010.
5. Windham-Myers L., W.-J. Cai, S. R. Alin, A. Andersson, J. Crosswell, K. H. Dunton, J. M. Hernandez-Ayon, M. Herrmann, A. L. Hinson, C. S. Hopkinson, J. Howard, X. Hu, S. H. Knox, K. Kroeger, D. Lagomasino, P. Megonigal, R. G. Najjar, M.-L. Paulsen, D. Peteet, E. Pidgeon, K. V. R. Schäfer, M. Tzortziou, Z. A. Wang, and E. B. Watson, 2018: Chapter 15: Tidal wetlands and estuaries. In Second State of the Carbon Cycle Report (SOCCR2): A Sustained Assessment Report [Cavallaro, N., G. Shrestha, R. Birdsey, M. A. Mayes, R. G. Najjar, S. C. Reed, P. Romero-Lankao, and Z. Zhu (eds.)]. U.S. Global Change Research Program, Washington, DC, USA, pp. 596-648, <https://doi.org/10.7930/SOCCR2.2018.Ch15>
6. Frankenberg C., Berry J. Solar Induced Chlorophyll Fluorescence: Origins, Relation to Photosynthesis and Retrieval; Elsevier: Amsterdam, The Netherlands, 2018; ISBN 9780124095489.
7. Mohammed G. H., Colombo R., Middleton, E. M., Rascher U., van der Tol C., Nedbal L., Goulas Y., Pérez-Priego O., Damm A., Meroni M., Joiner J., Cogliati S., Verhoef W., Malenovsky Z., Gastellu-Etchegorry J.-P., Miller J. R., Guanter L., Moreno J., Moya I., Berry J.A., Frankenberg C., Zarco-Tejada P. J. 2019. Remote sensing of solar-induced chlorophyll fluorescence (SIF) in vegetation: 50 years of progress. *Remote Sensing of Environment*, 231, 111177.
8. Porcar-Castell A., Tyystjärvi E., Atherton J., Tol C., Flexas J., Pfündel E.E., Moreno J., Frankenberg C., and Berry J.A. 2014. Linking chlorophyll a fluorescence to photosynthesis for remote sensing applications: mechanisms and challenges. *J. Exp. Bot.* 65(15), 4065–4095.
9. Yang X., Tang J., Mustard J.F., Lee J., Rossini M., Joiner J., Munger J.W., Kornfield A., Richardson A.D. 2015. Solar-induced chlorophyll fluorescence that correlates with canopy photosynthesis on diurnal and seasonal scales in a temperate deciduous forest. *Geophys. Res. Lett.* 42, 2977–2987.
10. Rossini M., Meroni M., Celesti M., Cogliati S., Julitta T., Panigada C., Rascher U., Van der Tol C., Colombo R. 2016. Analysis of red and far-red sun-induced chlorophyll fluorescence and their ratio in different canopies based on observed and modeled data. *Remote Sensing*, 8(5), 412; <https://doi.org/10.3390/rs8050412>.
11. Behrenfeld M.J., Westberry T.K., Boss E.S., O'Malley R.T., Siegel D.A., Wiggert J.D., Franz B.A., McClain C.R., Feldman G.C., Doney S.C., Moore J.K., Dall'Olmo G., Milligan A.J., Lima I., Mahowald N.

2009. Satellite-detected fluorescence reveals global physiology of ocean phytoplankton. *Biogeosciences*, 6, 779-794.
12. Yang X., Shi H., Stovall A., Guan K., Miao G., Zhang Y., Zhang Y., Xiao X., Ryu Y., L J-E. 2018. FluoSpec 2—an automated field spectroscopy system to monitor canopy solar-induced fluorescence. *Sensors*, 18(7), 2063. <https://doi.org/10.3390/s18072063>.
13. Perez-Priego, O., P. J. Zarco-Tejada, J. R. Miller, G. Sepulcre-Canto, and E. Fereres. 2005. Detection of water stress in orchard trees with a high-resolution spectrometer through chlorophyll fluorescence in-filling of the O2-A band, *IEEE Trans. Geosci. Remote Sens.*, 43(12), 2860–2869.
14. Burkart A., Schickling A., Mateo M. P. C., Wrobel T. J., Rossini M., Cogliati S., Julitta T., Rascher, U. (2015). A Method for Uncertainty Assessment of Passive Sun-Induced Chlorophyll Fluorescence Retrieval Using an Infrared Reference Light. *IEEE Sensors Journal*, 15(8), 4603–4611.
15. Webb E.K., Pearman G.I., Leuning R. 1980. Correction of flux measurements for density effects due to heat and water vapour transfer. *Q J R Meteorol Soc* 106: 85–100.
16. Aubinet M., Vesala T., Papale D. 2012. Eddy covariance: a practical guide to measurement and data analysis. Springer Science. ISBN 978-94-007-2350-4.